Wang, H. and Chen, Q. 2012. "A new empirical model for predicting single-sided, wind-driven natural ventilation in buildings," *Energy and Buildings*, 54, 386-394.

A New Empirical Model for Predicting Single-Sided, Wind-Driven Natural Ventilation in Buildings

Haojie Wang[1] and Qingyan Chen[1, 2*]
[1] School of Mechanical Engineering, Purdue University, West Lafayette, IN 47907, USA
[2] School of Environmental Science and Engineering, Tianjin University, Tianjin 300072, China
*Phone: (765) 496-7562, FAX: (765) 496-0539, Email: yanchen@purdue.edu

Abstract

Prediction of single-sided natural ventilation is difficult due to the bi-directional flow at the opening and the complex flow around buildings. A new empirical model was developed that can predict the mean ventilation rate and fluctuating ventilation rate due to the pulsating flow and eddy penetration of single-sided, wind-driven natural ventilation in buildings. The governing equation is based on the non-uniform pressure distribution along the opening height. The new model shows that the ventilation rate and wind velocity are linearly correlated. This investigation studied the eddy penetration effect in the frequency domain based on fast Fourier transform. Large Eddy Simulation (LES) and experimental data were used to validate the new empirical model. The model has also been used to analyze the influence of the opening geometry and elevation on the ventilation rate.

Key words: single-sided, wind-driven, natural ventilation, modeling

Nomenclature

A	Area	x	X position
C_d	Discharge coefficient	z	Z position
C_p	Pressure Coefficient	z_0	Z position of the neutral plane
H	Opening height		
k	Wave number	σ	Root mean square (RMS)
l	Opening width	υ	Viscosity
n	Frequency	θ	Wind incident angle
P	Pressure		
Q	Mean flow rate	Subscript	
Q_{in}	Inflow rate	//	Parallel to the opening
Q_{out}	Outflow rate	$\perp$	Normal to the opening
q	Fluctuating flow rate	e	Eddy penetration

S	Power spectrum	eff	Effective
S_{ij}	Strain rate tensor	i	Internal
T	Temperature	p	Pulsating flow
t	Time	ref	Reference value at 10 m
U	Instantaneous speed	w	Wind
$\overline{U}$	Mean Speed	Superscript	
u	Fluctuating speed	Tilt	In frequency domain

1 Introduction

Buildings use 40% of the primary energy in the United States, with a significant part of this energy being used to cool buildings [1]. As green buildings are becoming a trend in building design, natural ventilation has been drawing much attention in recent years for its ability to provide good thermal comfort [2] and indoor air quality [3] while utilizing a minimum amount of energy compared to that of mechanical ventilation. Natural ventilation can usually be classified into cross ventilation and single-sided ventilation. Cross ventilation is often favored for its larger air exchange rate than single-sided ventilation. However, in most cases, few buildings can achieve cross-ventilation due to the interior partitions, obstacles, and thicknesses. Therefore, single-sided ventilation is still of great importance in building design.

The major characteristics of single-sided ventilation are the fluctuating effect and the bi-directional flow at the opening. Among early studies, Warren [4] gave rather simple equations for wind- and buoyance-driven natural ventilation as

$$Q_{stack} = \frac{1}{3} A_{eff} C_d \sqrt{\frac{\Delta T H g}{T_{ave}}} \tag{1}$$

$$Q_w = 0.025 A_{eff} U_w \tag{2}$$

where C_d is 0.6, A_{eff} is the effective opening area, Q_{stack} is the buoyancy-driven ventilation rate, and Q_w is the wind-driven ventilation rate. The equation for wind-driven natural ventilation is an empirical correlation and has been used to provide a baseline for natural ventilation design. Phaff and De Gids [5] developed a semi-empirical correlation considering the mean, fluctuating flow, and buoyance effect as shown in Eq. (3)

$$U_{eff} = \sqrt{C_1 U_w^{\ 2} + C_2 H \Delta T + C_3} \tag{3}$$

where C_1, C_2 and C_3 are empirical constants. The effective velocity U_{eff} is used to calculate the ventilation rate via Eq. (4).

$$Q = 0.5 A U_{eff} \tag{4}$$

The coefficient of 0.5 in Eq. (4) is based on the assumption that each incoming and outgoing flow consists of half of the opening area.

Larsen and Heiselberg [6] developed a similar semi-empirical equation with additional consideration of different wind directions as

$$U_{eff} = \sqrt{C_1 f(\theta)^2 \left|C_p\right| U_{ref}{}^2 + C_2 H \Delta T + C_3 \frac{\Delta C_p \Delta T}{U_{ref}{}^2}} \quad (5)$$

where $f(\theta)$ is the function of wind incident angle determined experimentally and ΔC_p is the largest measured deviation of the C_p at the opening. They found that the wind direction had an unclear effect on the single-sided ventilation rate. A recent experimental investigation conducted by Caciolo et al. [7] examined the three models mentioned above and found that the simplest of Warren's equations gave the best overall results. However, the accuracy of all the equations is not very satisfactory and a major difficulty with the above correlations is the prediction of the fluctuating ventilation rate.

The fluctuating ventilation rate is the result of pulsating flow and eddy penetration. Haghighat et al. [8] studied the pulsating flow into a building when the wind was normal to the opening. They developed an equation for predicting a fluctuating ventilation rate in the frequency domain. The governing equation was based on Newton's Second Law. Linearization on the governing equation was made to use Fourier transform. The results calculated by the model show a good agreement with the experimental data. However, the model is limited to a condition in which the wind is normal to the opening and the assumption that a fluctuating velocity probability obeys a normal distribution. Eddy penetration is dominant when the wind is parallel to the opening [9]. Malinowski [10] suggested that only an eddy scale smaller than the opening scale can penetrate into a room. For studies on eddy penetration, there has been no quantitative analysis according to our recent literature review.

It is also hard to perform experimental measurements of single-sided ventilation, and the measured data is often of poor consistency. Since single-sided ventilation is largely influenced by the fluctuating wind velocity, the tracer-gas decay method is not suitable because it can only be used for steady state conditions. Another way is to measure the velocity distribution at the opening. However, for typical velocity measurements, such as hot wire anemometry, the equipment size will pose a limitation on the number of positions that can be measured [11]. Though advanced velocity measurement techniques such as laser Doppler anemometry can measure the velocity from a distance, they can only detect the velocity at one point each time and the equipment is usually very expensive [12]. Due to the random structure of wind, experimental measurements using particle imaging velocimetry would not yield meaningful results. Therefore, many researchers use Computational Fluid Dynamics (CFD) as an alternative to study single-sided ventilation. Jiang and Chen [13] used a Large Eddy Simulation (LES) model to calculate the ventilation rate and their results agreed well with the experimental data from Dascalaki et al. [14]. LES models are superior to Reynolds Averaged Navier-Stokes equation (RANS) models in single-sided ventilation because LES solves Navier-Stokes equations directly for eddies larger than the subgrid scale and they can capture the flow detachment and reattachment at the edge of the building enclosure, while RANS models generally cannot. However, CFD needs very detailed information about the buildings and the

computing cost can be very high. Thus, CFD is not used for initial and conceptual designs of natural ventilation.

This investigation intended to develop a new empirical model for predicting both the mean and fluctuating ventilation rate and the bi-direction velocity profile at the opening for single-sided wind driven ventilation. The model should consider the eddy penetration effect on the ventilation rate. The intention is to use the model for the initial and conceptual design. Our study will also quantify the influence of eddy penetration on ventilation rate and validate the model by LES simulations.

2 Empirical Model Development

The model developed in this investigation consists of three parts: (1) ventilation rate due to mean airflow, (2) fluctuating ventilation rate contributed by pulsating flow, and (3) fluctuating ventilation rate due to eddy penetration.

2.1 Ventilation rate due to mean airflow

For a room with a single opening, bi-directional flow will occur at the opening. The inflow and outflow are governed by the non-uniform wind pressure distribution along the opening height, as indicated by Figure 1. The wind pressure on the opening is

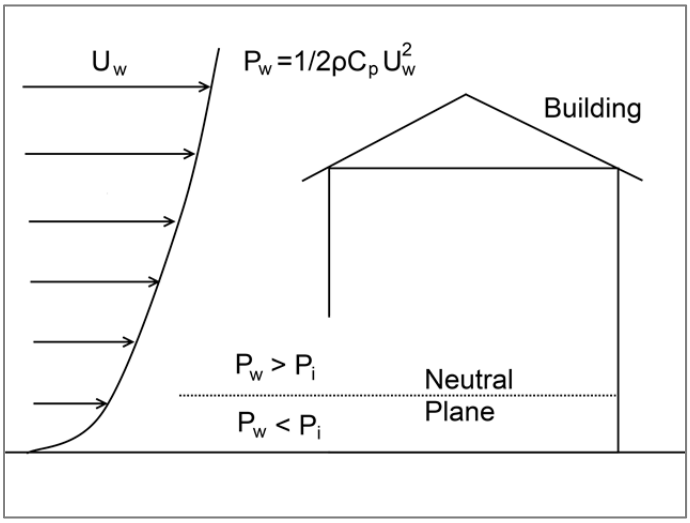

Figure 1 Bi-directional flow for wind driven single-sided ventilation

$$P_w(z) = \frac{1}{2} C_p U(z)^2 \tag{6}$$

The pressure coefficient C_p on the opening can be considered constant since the opening size is quite small compared to the building façade. Therefore, the wind pressure is only a function of the wind velocity. The wind velocity profile in the atmospheric boundary layer can be represented by the power law equation [15] as

$$\overline{U}(z) = \overline{U}_{ref}\alpha\left(\frac{z}{z_{ref}}\right)^{\gamma} \quad (7)$$

where α and γ [16] are listed in

Table 1. In this study, α is assumed to be 1.0 and Y to be 0.14, since we considered only flat terrains.

Table 1 Wind profile for different terrains

Terrain	α	γ
Flat terrains with a few trees or small buildings	1	0.14
Rural areas	0.85	0.20
Urban areas, industrial areas or forests	0.67	0.25
Large cities	0.47	0.35

The pressure difference that causes flow across the opening is

$$\Delta P(z) = \frac{1}{2} C_p U(z)^2 - P_i \tag{8}$$

where internal pressure can be calculated at the neutral plane (at z_0) as

$$P_i = \frac{1}{2} \rho C_p U(z_0)^2 \tag{9}$$

By using the orifice model, the inflow rate can be calculated as:

$$Q_{in} = \int_{z_0}^{h} C_d l \sqrt{\frac{2\Delta P(z)}{\rho}} dz \tag{10}$$

The outflow rate is:

$$Q_{out} = \int_{0}^{z_0} C_d l \sqrt{-\frac{2\Delta P(z)}{\rho}} dz \tag{11}$$

According to mass balance at the opening

$$Q = Q_{in} = Q_{out} \tag{12}$$

By combining Eqs. (7) - (12), then we have

$$Q = \frac{C_d l \sqrt{C_p} \int_{z_0}^{h} \sqrt{z^{2/7} - z_0^{2/7}} dz}{z_{ref}^{1/7}} U \tag{13}$$

The wind velocity can be decomposed into mean and fluctuating velocity as

$$U = \overline{U} + u \tag{14}$$

Then, we have the ventilation rate due to mean flow as:

$$\overline{Q} = \frac{C_d l \sqrt{C_p} \int_{z_0}^{h} \sqrt{z^{\frac{2}{7}} - z_0^{\frac{2}{7}}}\, dz}{z_{ref}^{1/7}} \overline{U} \tag{15}$$

2.2 Fluctuating ventilation rate contributed by pulsating flow

By combining Eqs. (13) and (14), we can obtain Eq. (16) for fluctuating ventilation rate due to pulsating flow,

$$\sigma_{q_p}{}^2 = \left(C_d l \frac{1}{z_{ref}^{1/7}} \sqrt{C_p} \int_{z_0}^{h} \sqrt{z^{2/7} - z_0^{2/7}}\, dz \right)^2 \sigma_u{}^2 \tag{16}$$

where σ_{q_p} is the fluctuating ventilation rate due to pulsating flow.

2.3 Fluctuating ventilation rate due to eddy penetration

As indicated by Straw et al. [9], Malinowsski [10], and Haghighat et al. [17], the fluctuating ventilation rate is also influenced by the eddy penetration but the impact has not been quantified. Malinowski [10] demonstrated that only an eddy with a scale smaller than the opening size can penetrate into the room. For natural ventilation, the outdoor wind contains eddies of different sizes, ranging from several hundred meters to micrometers [18]. Determining and filtering the eddies by their size needs spatial spectrum analysis of the wind velocity. Spatial spectrum is very difficult to obtain directly, but it can be calculated from the temporal spectrum. By assuming the outdoor wind as a homogenous turbulent flow, the Taylor Frozen hypothesis can be applied so that the temporal spectrum can be converted to a spatial spectrum via

$$S(k) = S(n) = \overline{U} \int_0^{\infty} S(\tilde{n}) d\tilde{n} \tag{17}$$

where $k = n / \overline{U}$.

As shown in Eq. (13), the ventilation rate is linearly proportionate to the wind velocity; therefore, it is reasonable to expect that the linearity still exists for the spectra of wind velocity and ventilation rate. The governing equation for the eddy penetration rate in the frequency domain thus is

$$\widetilde{q_e} = CA\widetilde{u_{//}} \tag{18}$$

where $C = C_d \sqrt{C_p} / 2$ and $\widetilde{u_{//}}$ is the fluctuating velocity parallel to the opening in the frequency domain.

The spectrum of velocity can then be correlated to the root mean square (RMS) of the eddy penetration rate (fluctuating ventilation rate due to eddy penetration) as

$$\sigma_{q_e}{}^2 = C^2 A^2 \overline{U} \int_{\overline{U}/l}^{\infty} S(\tilde{n}) d\tilde{n} \tag{19}$$

The lower and upper limits of the integral represent the size of the penetrated eddies.

Furthermore, the total RMS of the ventilation rate (fluctuating ventilation rate due to both pulsating flow and eddy penetration) is calculated from

$$\sigma_q = \sqrt{\sigma_{q_e}{}^2 + \sigma_{q_p}{}^2} \tag{20}$$

Thus, we have developed empirical models for predicting the mean ventilation rate and fluctuating ventilation rate for single-sided wind driven ventilation as Eq. (15) and Eq. (20), respectively.

3 CFD Model

This investigation performed several CFD simulations for different wind conditions to generate high fidelity data for validating the empirical models developed. The CFD simulations used LES to study single-sided ventilation due to its better accuracy than the RANS models [13]. LES filters the flow by eddy scales and resolves the Navier-Stokes equation directly for eddies larger than the scale. To filter a flow variable, ϕ, by using a filter function, G, the filtered variable $\overline{\phi}$ is

$$\overline{\phi}(x) = \int_D \phi(x') G(x, x') dx' \tag{21}$$

Our study used numerical grid size as the filter size. The filtered Navier-Stokes equation is (the over bars in this section represent filtered variables)

$$\frac{\partial \overline{u_i}}{\partial t} + \frac{\partial \overline{u_i}\,\overline{u_j}}{\partial x_j} = -\frac{1}{\rho}\frac{\partial \overline{p}}{\partial x_i} + 2\upsilon \frac{\partial}{\partial x_j}\overline{S_{ij}} - \frac{\partial \tau_{ij}^r}{\partial x_j} \tag{22}$$

where τ_{ij}^r is the residual stress tensor that needs to be modeled. S_{ij} is the strain rate tensor:

$$\overline{S_{ij}} = \frac{1}{2}\left(\frac{\partial \overline{u_i}}{\partial x_j} + \frac{\partial \overline{u_j}}{\partial x_i}\right) \tag{23}$$

This study correlated τ_{ij}^r with the strain rate tensor by the Boussinesq hypothesis

$$\tau_{ij}^r - \frac{1}{3}\tau_{kk}\delta_{ij} = -2\upsilon_{SGS}\overline{S_{ij}} \tag{24}$$

The isotropic part τ_{kk} is zero for incompressible flow; thus, the residual stress tensor is simply proportional to the strain rate tensor. The ν_{SGS} is the subgrid scale turbulence viscosity defined by the Smagorinsky-Lilly model [19] as

$$\upsilon_{SGS} = (C_{SGS}\Delta)^2 \sqrt{2\overline{S_{ij}}\,\overline{S_{ij}}} \tag{25}$$

where C_{SGS} is the Smagorinsky constant and Δ is the grid scale.

The pressure velocity coupling scheme used is SIMPLE. The momentum discretization scheme is the bounded central differencing and for the temporal discretization, the second order implicit method is used [20]. The LES was used to generate accurate flow data for validating the new empirical models.

4 Results and Discussion

4.1 Case setup

This investigation used LES to calculate five cases of single-sided natural ventilation. The simulations needed fluctuating wind velocity in the inlet boundary conditions, which were generated by synthesizing a divergence-free velocity field from the summation of Fourier harmonics [21,22]. Figure 2 compares the instantaneous velocity generated by the method with the mean wind velocity.

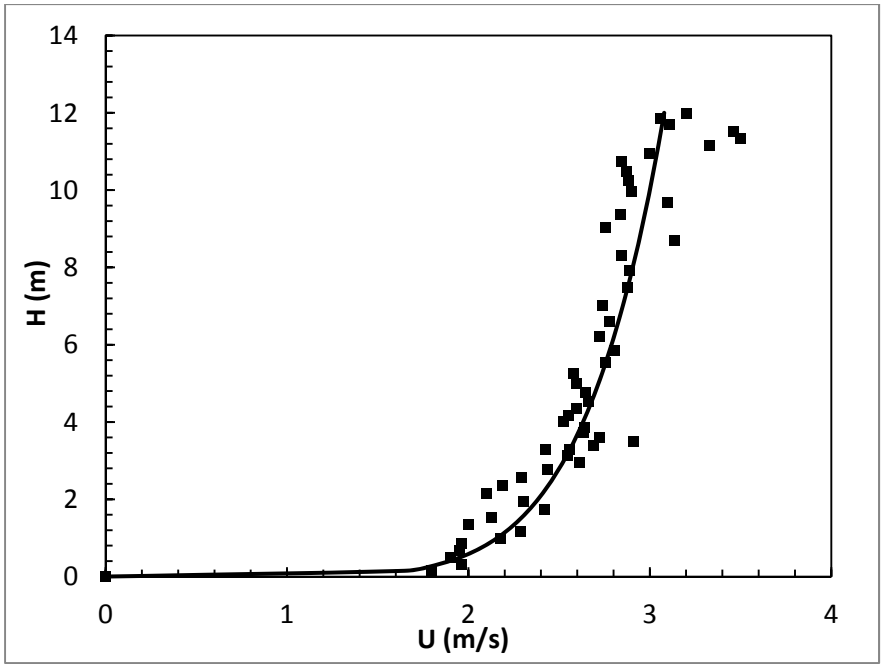

Figure 2 Transient velocity (black squares) and mean velocity (solid line) at the inlet for LES

Our study used the building geometry from [14] for the CFD simulations. The building dimension was 3.6×2.4×3.3 (m^3) with an opening of 1×2 (m^2) as shown in

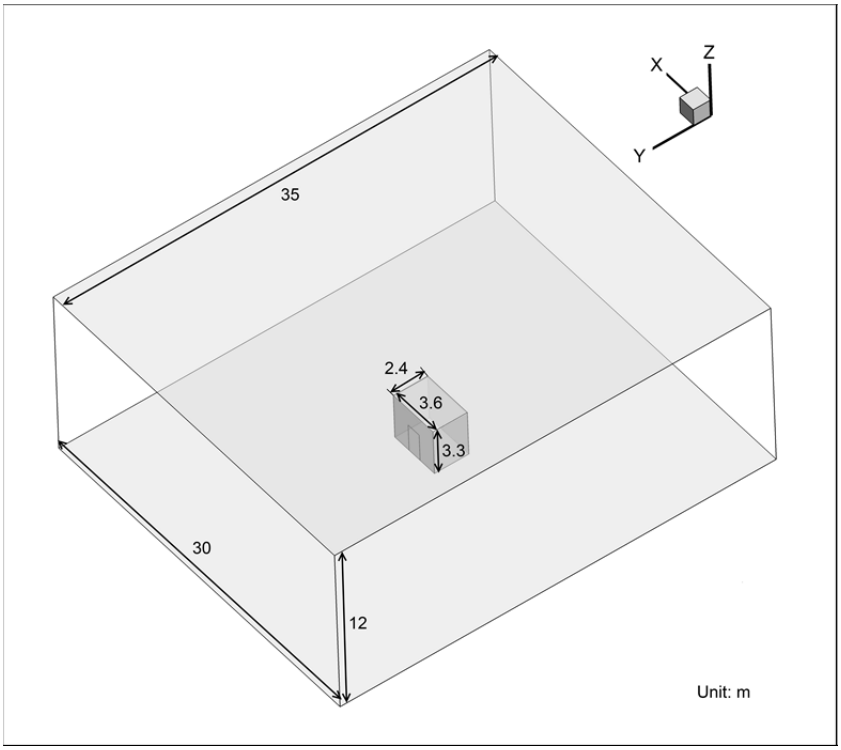

Figure 3. The computing domain was much larger than the building to obtain a fully developed flow and for better convergence.

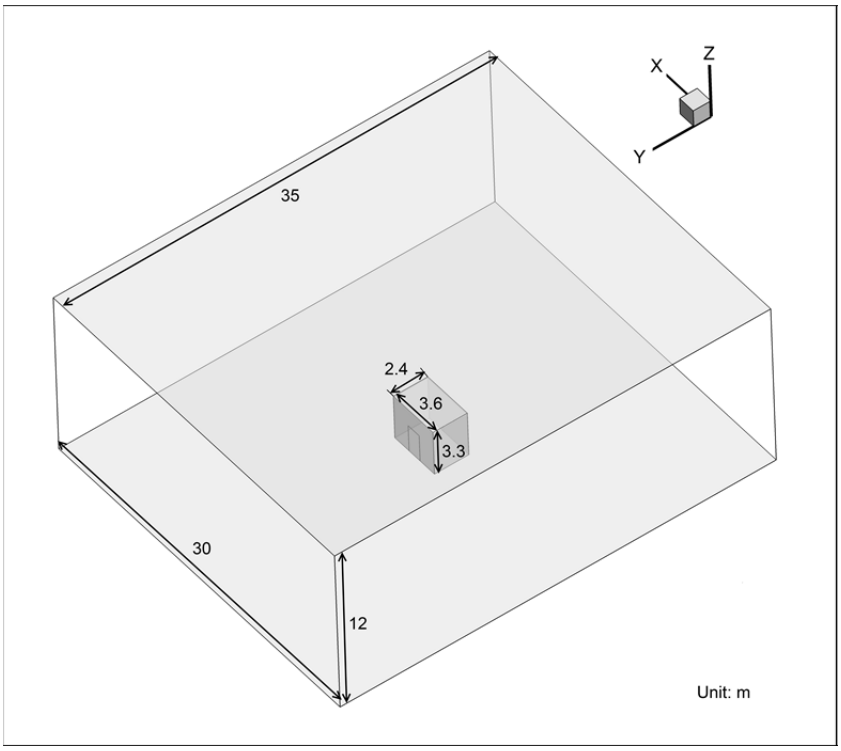

Figure 3 CFD domain and building geometry

Table 2 summarizes the cases studied where the first five cases used the building geometry from Dascalaki et al. [14] and two of them had experimental data. Our investigation first compared the CFD simulation results (Q_{CFD}) with the experimental data (Q_{exp}) from Dascalaki et al. [14] for Cases 1 and 2. Since the ventilation rates calculated by CFD were similar to those measured, CFD was further used to generate three more cases (Cases 3, 4, and 5) for a room with different wind velocity and direction. Cases 6 and 7 were from the experiment conducted by Caciolo et al. [7], and only the wind dominant cases from their data were chosen to compare with the predicted results. The room geometry for Cases 6 and 7 was $3\times3.5\times2.5$ (m^3) on the second floor of a building and the opening size for the room was 1×1 (m^2). Since their study did not provide sufficient information about the whole building, we could not perform CFD simulations for the two cases. However, the experimental data can be used to compare with the data calculated by the new empirical models.

Table 2 Comparison of predicted, measured, and CFD calculated ventilation rates

	$\overline{U}_{ref}$	θ	Q_{pred}	Q_{CFD}	Q_{exp}	σ_{q_e}	σ_{q_p}	$\sigma_{q_{pred}}$	$\sigma_{q_{CFD}}$
Case1	2.05	68	0.0555	0.0602	0.0540	0.0143	0.0083	0.0166	0.0166
Case2	2.59	60	0.1020	0.0791	0.0914	0.0278	0.0178	0.0330	0.0263
Case3	3.00	90	0.3600	0.3405	-	0.1025	0.0541	0.1159	0.1403
Case4	3.00	30	0.3647	0.3750	-	0.0414	0.0548	0.0687	0.0672
Case5	3.00	0	0.4729	0.4636	-	-	0.0711	0.0711	0.0840
Case6	3.9	152	0.1118	-	0.0882	-	-	-	-
Case7	3.4	145	0.0975	-	0.0802	-	-	-	-

4.2 Comparison of the ventilation rates determined by different methods

Cases 1 and 2 in Table 2 show that the difference is less than 15% between the ventilation rates measured and those calculated by CFD. This proves that the CFD simulations were accurate and reliable. Also, Q_{exp} and Q_{CFD} were compared with the empirical model result, Q_{pred}. The three values agree with each other well. Furthermore, CFD simulation can obtain the fluctuating ventilation rate, $\sigma_{q_{CFD}}$, which can be compared with that calculated by the empirical model. For the empirical model, the fluctuating ventilation rate, $\sigma_{q_{pred}}$, is the square root sum of the eddy penetration rate, σ_{q_e}, and pulsating flow, σ_{q_p}. Table 2 lists the three components, and $\sigma_{q_{pred}}$ agrees well with $\sigma_{q_{CFD}}$.

Cases 3, 4, and 5 were for different wind directions. The mean and fluctuating ventilation rates calculated by CFD were compared with those by the empirical models, and the agreement between them was good. Cases 6 and 7 have only measured mean ventilation rate since the building information was insufficient to perform CFD simulations. The differences between the measured data and the empirical predictions were slightly larger than in the other cases because the opening was at the leeward side where the flow field near the opening was much more complicated.

The wind direction has a large influence on ventilation rate. When the wind incident angle is around 70^{o}, the absolute value of the pressure coefficient approaches to zero. According to Eqs. (15), (16), and (19), both the mean and fluctuating ventilation rates were much smaller than those when the wind was normal or parallel to the opening. When the wind direction was parallel to the opening, eddy penetration was dominant in the fluctuating ventilation rate, as shown in Case 3. When the wind direction was normal to the opening, there was no eddy penetration and the fluctuating ventilation rate was only caused by the pulsating flow. The fluctuating ventilation rate when the wind was parallel to the opening should be larger than the rate when the wind was normal to the opening, due to the stronger turbulence effect.

Figure 4 correlates all the predicted results by the empirical model with the CFD and experimental data. The squares represent the mean ventilation rate and the triangles stand for the fluctuating ventilation rate. The figure shows that the predicted values by the empirical models were generally within ±20% error bars of the measured data or CFD results.

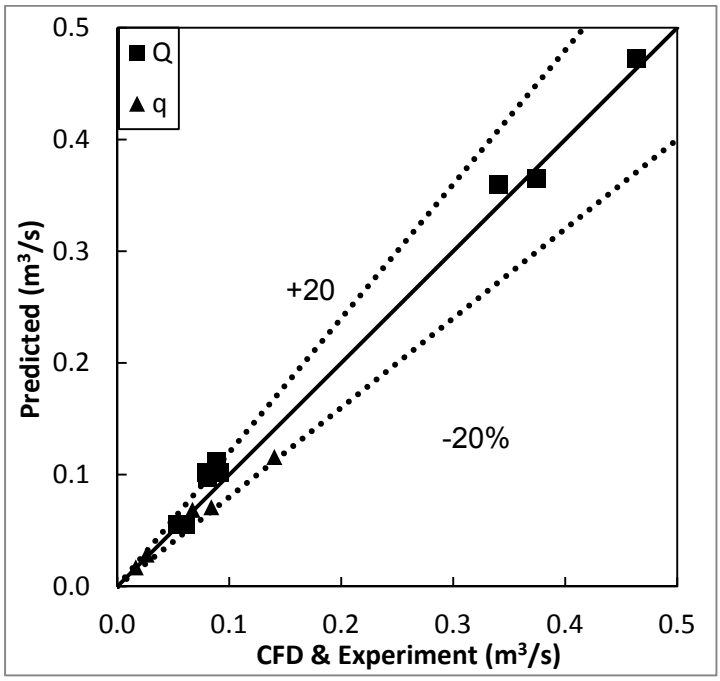

Figure 4 Comparison of predicted ventilation rate with CFD and measured ventilation rate

4.3 Impact of eddy penetration on fluctuating ventilation rate

Figure 5 illustrates the impact of eddy penetration in the frequency domain on the ventilation rate. Figure 5(a) shows the fluctuating spectra of the ventilation rate when the wind was parallel to the opening (Case 3). The red line is the spectrum of the ventilation rate directly calculated from the CFD results, which can be considered as the actual fluctuating ventilation rate. The purple line is the spectrum of the ventilation rate calculated by Eq. (26) without considering the eddy penetration:

$$S_q(n) = \left(\frac{C_d l \sqrt{C_p} \int_{z_0}^{h} \sqrt{z^{\frac{2}{7}} - z_0^{\frac{2}{7}}}\, dz}{z_{ref}^{1/7}} \right)^2 S_u(n) \qquad (26)$$

where $S_u(n)$ is the fluctuating velocity spectrum at the inlet. The blue line is the spectrum of the ventilation rate calculated by Eq. (27), which includes the eddy penetration effect by

$$S_q(n)=\begin{cases}\left(\dfrac{C_d l\sqrt{C_p}\int_{z_0}^{h}\sqrt{z^{\frac{2}{7}}-z_0^{\frac{2}{7}}}\,dz}{z_{ref}^{1/7}}\right)^2 S_u(n) & when\ \ n<\overline{U}/l \\ \left(\dfrac{C_d l\sqrt{C_p}\int_{z_0}^{h}\sqrt{z^{\frac{2}{7}}-z_0^{\frac{2}{7}}}\,dz}{z_{ref}^{1/7}}\right)^2 S_u(n)+\left(\dfrac{AC_d\sqrt{C_p}}{2}\right)^2 S_{u_1}(n) & when\ \ n\geq\overline{U}/l\end{cases} \tag{27}$$

where $S_{u_1}(n)$ is the spectrum of the fluctuating velocity component that is parallel to the opening.

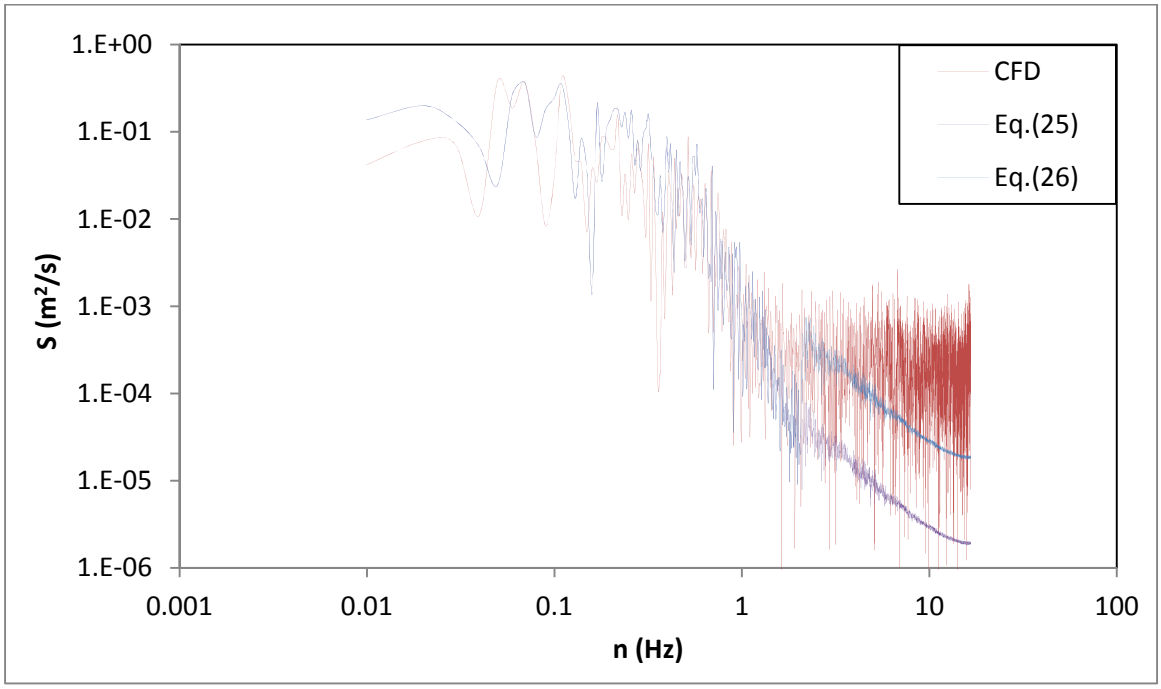

(a)

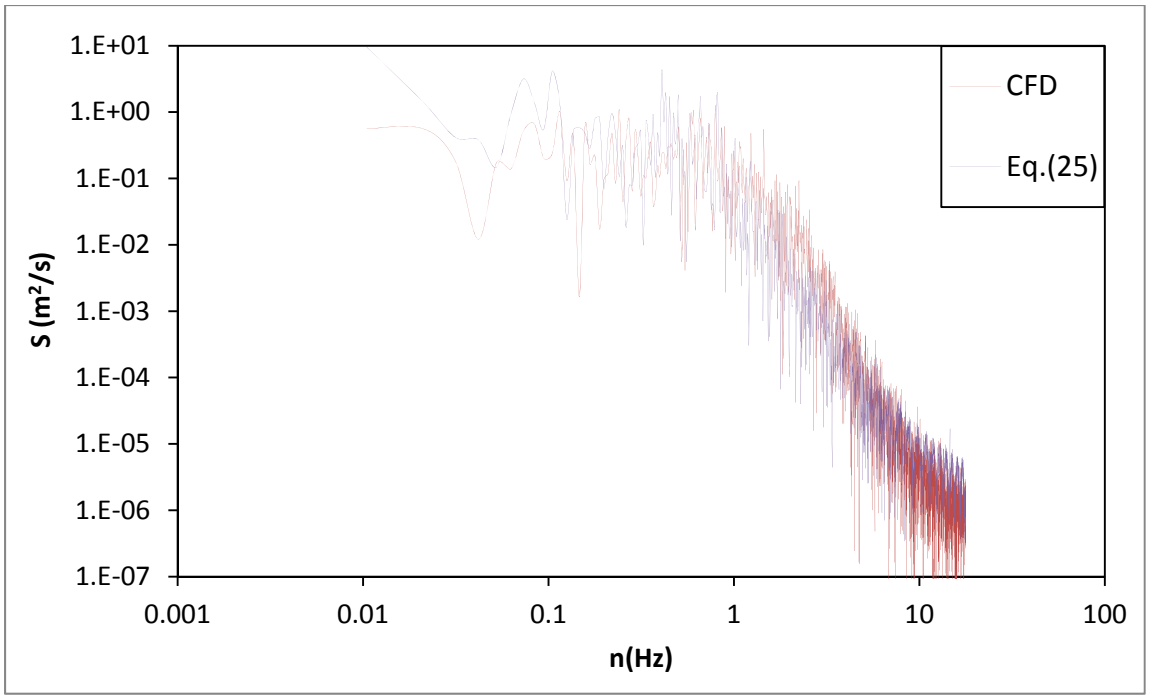

(b)

Figure 5 Spectra of the fluctuating ventilation rate (a) when the wind was parallel to the opening and (b) when the wind was normal to the opening

When the frequency is around 1, the corresponding eddy scale can penetrate into the opening. The results in Figure 5(a) indicate that, when the frequency is greater than 1, the red line will become much larger than the purple line. The difference is the energy of the penetrated eddies. When eddy penetration is considered, the blue line is closer to the red line (actual value). However, some discrepancies still exist because of the use of the Taylor Frozen hypothesis. This hypothesis is applied to convert the spectrum in the temporal domain into the spatial domain to filter the eddies based on their scales. It will lead to two problems: 1) the hypothesis assumes the flow is a homogeneous turbulent flow, which in this case may not be satisfied; 2) the mean velocity at the opening in Eqs. (19) and (27) was replaced by the mean wind velocity at the far field. Despite the two problems, this investigation used the Taylor Frozen hypothesis due to its simplicity and good overall accuracy.

Figure 5(b) shows the ventilation rate spectra when the wind is normal to the opening. The red line is the spectrum of the fluctuating ventilation rate calculated by CFD. The purple line is the spectrum of the ventilation rate calculated by Eq. (26) without considering the eddy penetration and agrees well with the CFD result. Compared with Figure 5(a), there was no eddy penetration when the wind was normal to the opening, which was consistent with the assumption made in Eq. (18).

4.4 Discussion

The model can predict the mean velocity component that is normal to the opening via

$$\overline{U_{\perp}}(z)=\begin{cases}\dfrac{C_d\sqrt{\left|C_p(z^{2/7}-z_0^{2/7})\right|}}{z_{ref}^{\ 1/7}}\overline{U}_{ref} & when\ C_p\cdot(z^{2/7}-z_0^{2/7})>0\\ -\dfrac{C_d\sqrt{\left|C_p(z^{2/7}-z_0^{2/7})\right|}}{z_{ref}^{\ 1/7}}\overline{U}_{ref} & when\ C_p\cdot(z^{2/7}-z_0^{2/7})\le 0\end{cases} \tag{28}$$

When $C_p\cdot(z^{2/7}-z_0^{2/7})>0$, the flow goes inwards to the building and when $C_p\cdot(z^{2/7}-z_0^{2/7})\le 0$, the flow goes outwards. As indicated by Eq.(28), when the pressure coefficient, C_p, is positive, the inflow will be in the upper part of the opening, and when it is negative, the inflow will be in the lower part of the opening.

This model assumes that the velocity along the opening width is the same. However, the results from CFD for Case 4 as shown in Figure 6(a) show that the velocity along the opening width is not uniform. Eq. (29) can be used to average the CFD results along the opening width to compare with those calculated by the empirical model:

$$\overline{U_{1\,ave}}(z)=\frac{\sum_k\left(\dfrac{\sum_i\overline{U}_{\perp}(t_i,x_k,z)}{\Delta t}\right)\Delta x_k}{l} \tag{29}$$

where k is the summation index through the opening width and Δt is the time period for the calculation. Then one can compare the velocity profile at the opening calculated by CFD with the profile by the empirical model.

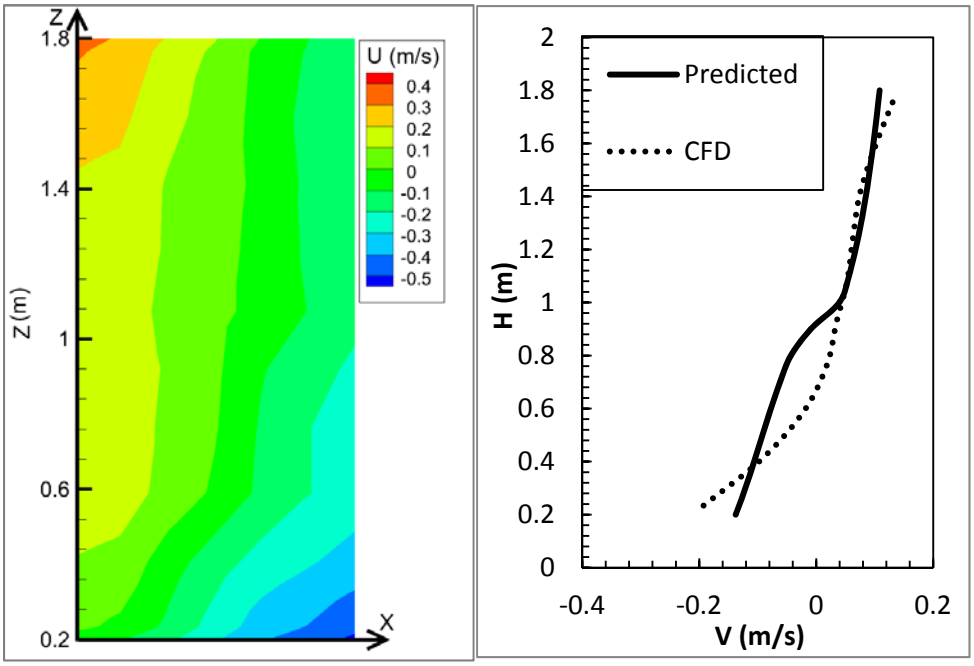

(a) (b)

Figure 6 (a) Y-velocity (normal to the opening) contour and (b) predicted Y-velocity profile versus averaged Y-velocity profile from CFD

Figure 6(b) compares the averaged velocity profile by CFD with that by the empirical model. In general, the two profiles are similar but with some differences in the lower part of the opening where the flow goes outwards. One possible reason is that the outflow will interact with the incoming wind and thus distort the flow field, which can be accounted for by CFD but not by the empirical model.

As mentioned in section 4.2, the wind direction will have a large influence on the ventilation rate. A more detailed analysis on the impact of wind direction on eddy penetration rate is necessary. Figure 7(a) shows the pressure coefficient for different wind directions. The pressure coefficient is normalized by the pressure coefficient when the incident angle is 90^o (the pressure coefficient for this case is negative). We selected 90^o because the eddy penetration rate is the largest. When the incident angle is smaller than 70^o, the normalized pressure coefficient is negative and the absolute value decreases as the incident angle increases. For an incident angle between 70º to 90º, the normalized pressure coefficient is positive and the absolute value increases as the incident angle increases. Note that the actual pressure coefficient will decrease monotonically with an increasing incident angle for windward cases because the wind load on the opening side reduces with the incident angle. For an incident angle larger than 90º, the pressure coefficient is around a certain value. This is mainly due to the weak zone at the leeward side [23,24].

Figure 7(b) depicts how the wind incident angle affects the eddy penetration. The eddy penetration rate is normalized by the penetration rate when the incident angle equals 90^o. According to Eq.(18), the two major factors that determine the eddy penetration rate are the

pressure coefficient and the parallel velocity component. The eddy penetration rate will increase with the absolute pressure coefficient and the parallel velocity. When the incident angle is smaller than 90^o, the parallel velocity will increase monotonically and yet the absolute pressure coefficient will first decrease and then increase. This will result in a dip of the eddy penetration rate at around 70^o where the pressure coefficient is close to zero. It should be noted that zero pressure coefficient may not exist in reality due to the fluctuation of the wind.

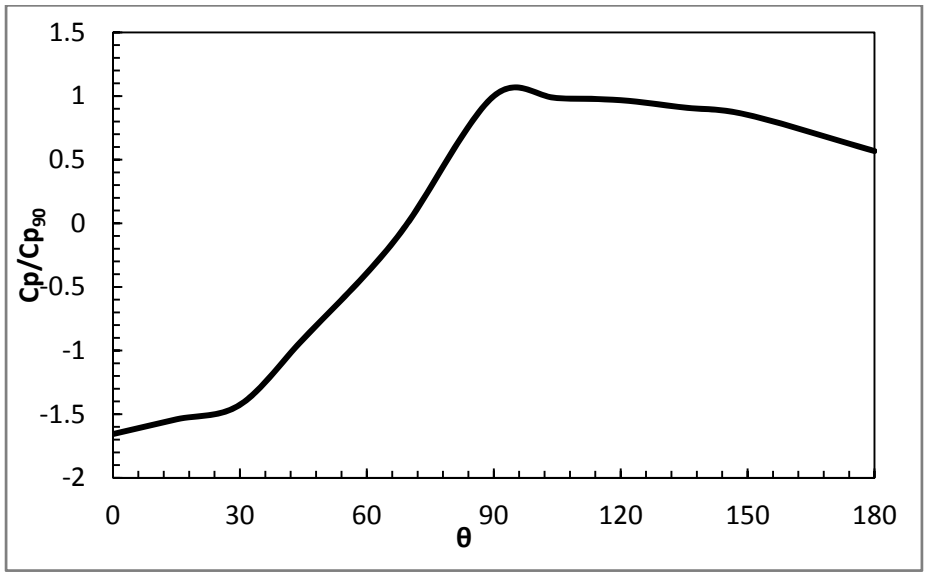

(a)

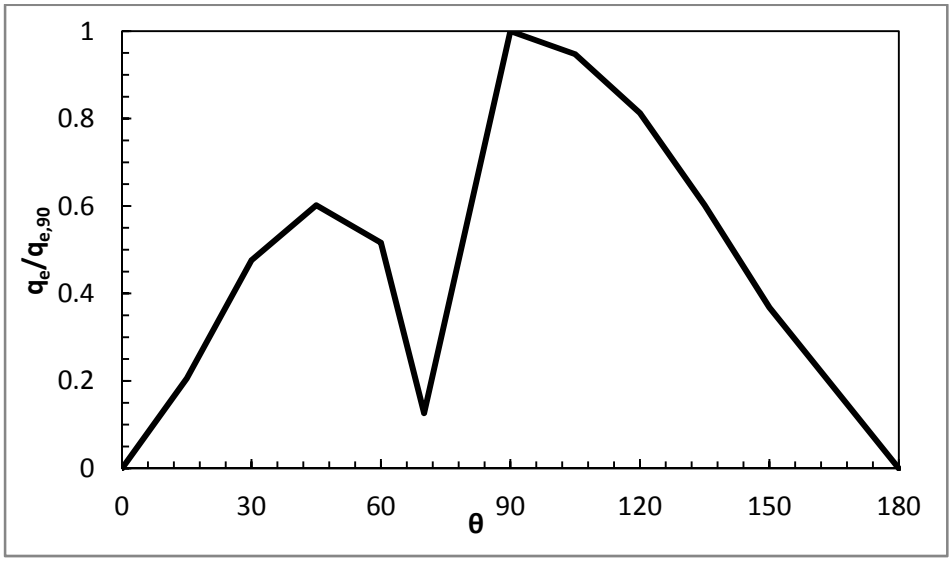

(b)

Figure 7 (a) Normalized pressure coefficient for different wind directions and (b) normalized eddy penetration rate for different wind directions

Other important factors influencing ventilation rate are the opening size and the elevation. The existing models for predicting ventilation rates often assume a linear relation between ventilation rate and opening size. Our model (Eqs. (15), (16), and (19)) shows that the opening height and width will result in non-linearity of the ventilation rate for single-sided ventilation. The effective velocity at the opening is defined as

$$U_{eff} = \frac{Q}{\frac{A}{2}} \tag{30}$$

where Q can be either mean ventilation rate or eddy penetration rate. Figure 8**Error! Reference source not found.** shows the influence of opening size on the effective velocity. The effective velocity is normalized by that of unit opening width or unit height. The solid line represents the effective eddy penetration velocity. As the opening width increases, the effective eddy penetration velocity also increases because more eddies can penetrate into the opening. Since the velocity spectrum variation is nonlinear, the effective velocity variation is also nonlinear, based on Eq. (19).

The dashed line represents the effective velocity changes with the opening height. As the opening height increases, the pressure difference along the opening height will increase. Pelletret et al. [25] conducted several experiments for single-sided ventilation and found a nonlinear increase in the ventilation rate with the opening height. Our model (Eq. (13)) indicates that as the opening height increases, the pressure difference along the opening height will increase. Thus, this will result in a nonlinear increase of the ventilation rate or effective velocity, which agrees well with the findings from Pelletret et al.

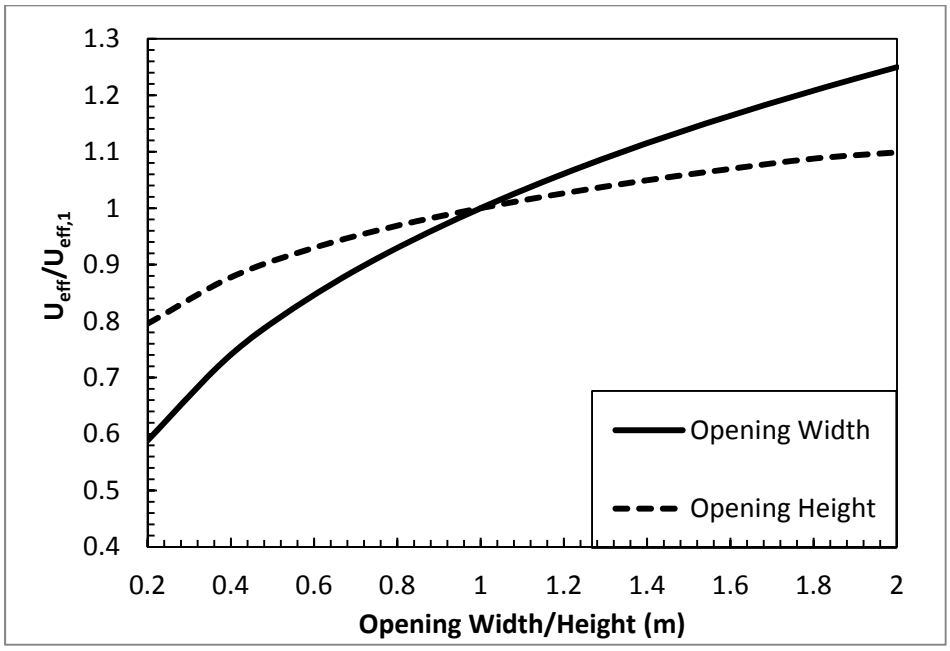

Figure 8 Normalized effective velocities for different opening widths and heights

The opening elevation to the ground can also influence the effective ventilation rate. As the elevation increases, the approaching wind velocity will also increase in the atmospheric boundary layer. Both an increase in wind velocity and elevation will have an influence on the ventilation rate. To differentiate the two factors, this investigation studied two cases: Elevation-1 and Elevation-2, as shown in Figure 9(a). Elevation-1 assumed an opening elevation change from 1 m to 2 m, but the wind velocity remained unchanged at 3.0 m/s. This is a case of changing wind profile as shown in the left figure of Figure 9(a). Elevation-2 changed the elevation but used the same wind profile so that the wind velocity at the opening would change. Figure 9(b) illustrates the impact of elevation on effective velocity for the two scenarios. The ventilation rate will decrease along with the elevation for both cases, due to the pressure decrease along the opening height. Scenario Elevation-2 has a higher ventilation rate than Scenario Elevation-1 because of the change of velocity in the opening.

Note that the above analysis is true for a building with only one opening. For single-sided ventilation with multiple openings, the result could be different since some openings will only have inflow and some will only have outflow. The governing force will be the wind pressure difference between each opening rather than the pressure difference along one opening height, as proposed in our models.

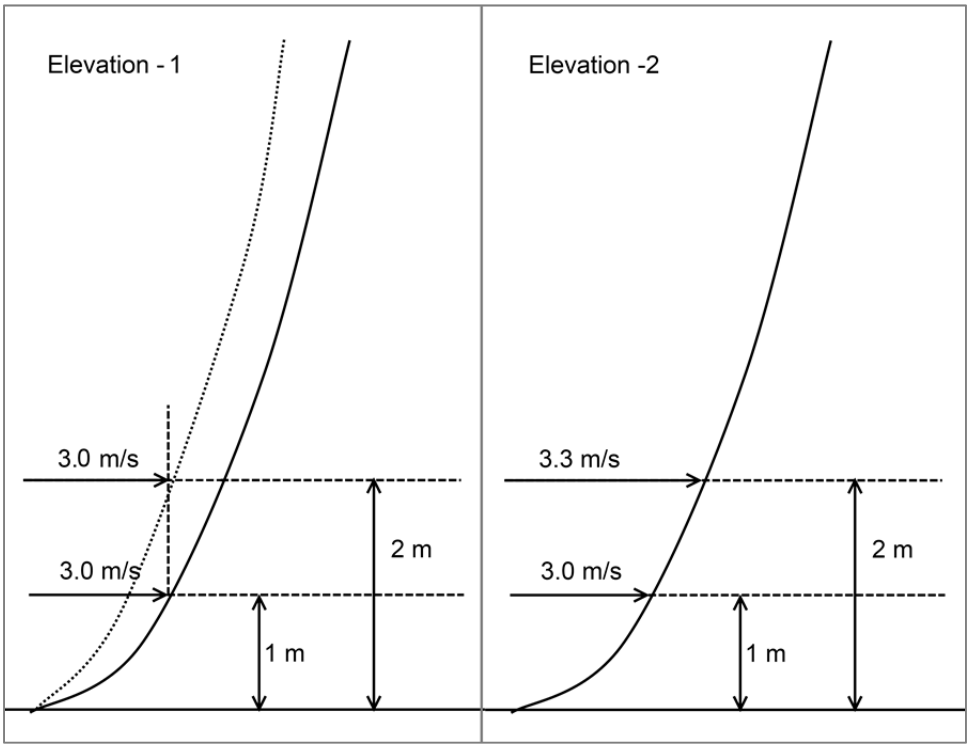

(a)

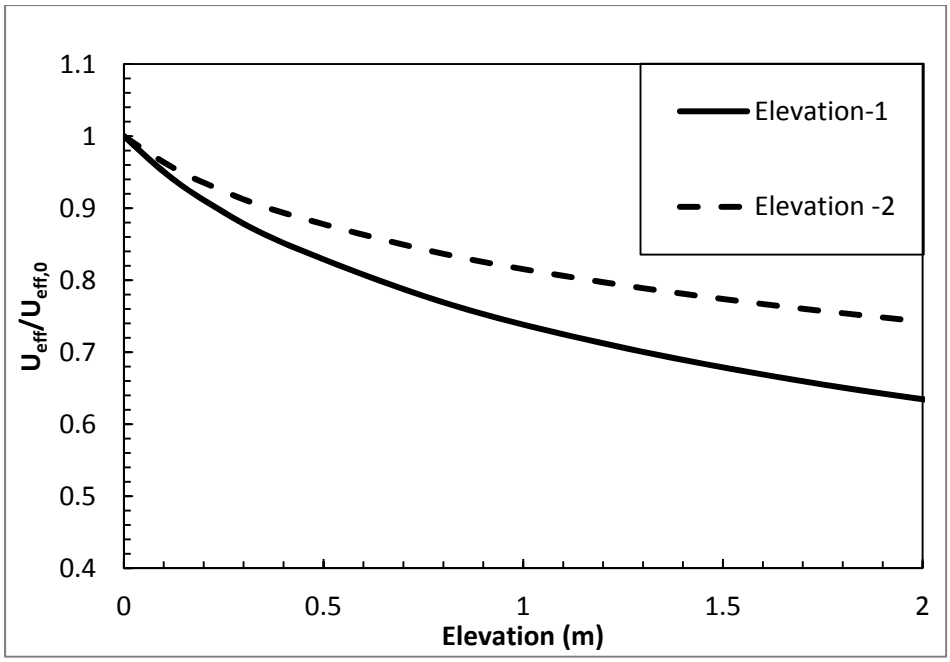

(b)

Figure 9 (a) The impact of opening elevation on ventilation rate (a) scenarios of elevation change and (b) normalized effective velocities for different elevations

5 Conclusion

This paper proposed new empirical models to predict a single-sided, wind-driven ventilation rate. The study led to the following conclusions:

1) Based on the pressure difference along an opening height, the empirical models can calculate the mean and the fluctuating ventilation rate through the opening. The fluctuating ventilation rate is a combination of pulsating flow and eddy penetration. This investigation used spectrum analysis to quantify the eddy penetration effect and has proved the eddy penetration to be a major factor when the wind is parallel to the opening.
2) CFD simulations of single-sided natural ventilation by LES were performed. The simulated results together with experimental data from the literature were used to validate the new empirical models. The differences between the empirical model predictions and CFD and/or the experimental data were less than 25%.
3) The profile of the normal velocity component at an opening can be predicted by our model, which also agrees with the CFD result.
4) This investigation also found that eddy penetration was zero when the wind incident angle was 0^o due to zero parallel velocity, and the penetration was low when the angle was around 70^o due to the low absolute pressure coefficient. The ventilation rate will

increase non-linearly with the opening size and will decrease as the opening elevation to the ground increases.

Acknowledgement

This research was supported by the U.S. Department of Energy through the Energy Efficient Buildings Hub.

6 References

[1] Energy information Agency, Annual Energy Review, 2011.

[2] ASHRAE Standard 55, Thermal environmental conditions for human occupancy, 2010.

[3] J. Finnegan, C. Pickering, and P. Burge, The sick building syndrome: prevalence studies, British Medical Journal 289 (1984) 1573-1575.

[4] P. Warren, Ventilation through openings on one wall only, in Energy conservation in Heating, Cooling and Ventilating, Dubrovnik, Yugoslavia, 1977.

[5] H. Phaff and W. De Gids, Ventilation rates and energy consumption due to open windows: a brief overview of research in the Netherlands, Air Infiltration Review 4 (1982) 4–5.

[6] T. Larsen and P. Heiselberg, Single-sided natural ventilation driven by wind pressure and temperature difference, Energy and Buildings 40 (2008) 1031–40.

[7] Marcello Caciolo, Pascal Stabat, and Dominique Marchio, Full scale experimental study of single-sided ventilation: analysis of stack and wind effects, Energy and Buildings 43 (2011) 1765-1773.

[8] F. Haghighat, J. Rao, and P. Fazio, The influence of turbulent wind on air change rates- a modeling approach, Building and Environment 26 (1991) 95-109.

[9] M. Straw, C. Baker, and A. Robertson, Experimental measurements and computations of the wind-induced ventilation of a cubic structure, Journal of Wind Engineering and Industrial Aerodynamics 88 (2000) 213-230.

[10] H. Malinowski, Wind effect on the air movement inside buildings, in Proceedings of the third international conference on wind on buildings and structures, Tokyo, 1971, 125-134.

[11] C. G. Lomas, Fundamentals of hot wire anemometry, Cambridge University Press, New York, 1986.

[12] Preben Buchhave and W. K. George Jr., The measurement of turbulence with the Laser-Doppler anemometer, Annual Review of Fluid Mechanics 11 (1979) 443-503.

[13] Yi Jiang and Qingyan Chen, Study of natural ventilation in buildings by large eddy simulation, Journal of Wind Engineering and Industrial Aerodynamics 89 (2001) 1155-1178.

[14] E. Dascalaki, M. Santamouris, and A. Argiriou, On the combination of air velocity and flow measurements in single sided natural ventilation configurations, Energy and Building 24 (1996) 155-165.

[15] G. Hellman, Uber die bewegung der luft in den untersten scichten der atmosphare, Meteorologische Zeitschrift 34 (1916) 273.

[16] M. Sherman and M. Modera, Comparison of measured and predicted infiltration using the LBL infiltration model, in Proceedings Measured Air Leakage of Buildings, Philadelphia, 1986, 325-347.

[17] F. Haghighat, Herik Brohus, and Jiwu Rao, Modeling air infiltration due to wind fluctuations – a review, Building and Environment 35 (2000) 377-385.

[18] Emil Simiu and Robert Scanlan, Wind Effects on Structures: An Introduction to Wind Engineering, Wiley-Interscience, New York,1986.

[19] Joseph Smagorinsky, General Circulation Experiments with the Primitive Equations, Monthly Weather Review 91 (1963) 99-164.

[20] ANSYS Inc., ANSYS FLUENT 12.0 Theory Guide, 2009.

[21] R. Kraichnan, Diffusion by a Random Velocity Field, Physics of Fluids 11 (1970) 21-31.

[22] R. Smirnov, S. Shi, and I. Celik, Random flow generation technique for large eddy simulations and particle-dynamics modeling, Journal of Fluids Engineering 123 (2001) 359-371,.

[23] G. Walton, Airflow and multiroom thermal analysis, ASHRAE Transactions 88 (1982) 78-91,.

[24] M. Swami and S. Chandra, Correlations for pressure distribution of buildings and calculation of natural-ventilation airflow, ASHRAE Transactions 94 (1988) 243-266.

[25] R. Pelletret, F. Allard, F. Haghighat, and J. Van der Maas, Modeling of large Openings, in Proceedings of 12th AIVC Conference, Ottawa, Canada, 1991.